Virology 492 (2016) 118–129

Contents lists available at ScienceDirect

Virology

journal homepage: www.elsevier.com/locate/yviro

Genetic characterization of an adapted pandemic 2009 H1N1 influenza virus that reveals improved replication rates in human lung epithelial cells

Xenia Wörmann [a,1], Markus Lesch [a,b,1], Robert-William Welke [c], Konstantin Okonechnikov [a], Mirshat Abdurishid [a], Christian Sieben [c,2], Andreas Geissner [d,e], Volker Brinkmann [a], Markus Kastner [f], Andreas Karner [g], Rong Zhu [f], Peter Hinterdorfer [f], Chakkumkal Anish [d,3], Peter H. Seeberger [d,e], Andreas Herrmann [c], Thomas F. Meyer [a,b], Alexander Karlas [a,b,*]

[a] Department of Molecular Biology, Max Planck Institute for Infection Biology, Berlin, Germany
[b] Steinbeis Innovation gGmbH, Center for Systems Biomedicine, Falkensee, Germany
[c] Department of Biology, Molecular Biophysics, IRI Life Sciences, Humboldt-Universität zu Berlin, Germany
[d] Department for Biomolecular Systems, Max Planck Institute for Colloids and Interfaces, Potsdam, Germany
[e] Institute of Chemistry and Biochemistry, Free University, Berlin, Germany
[f] Institute for Biophysics, Johannes Kepler University, Linz, Austria
[g] Center for Advanced Bioanalysis GmbH (CBL), Linz, Austria

ARTICLE INFO

Article history:
Received 13 November 2015
Returned to author for revisions
3 December 2015
Accepted 3 February 2016
Available online 23 February 2016

Keywords:
A/Hamburg/04/2009
Hemagglutinin
High-throughput sequencing
Reverse genetics
Viral adaptation

ABSTRACT

The 2009 influenza pandemic originated from a swine-origin H1N1 virus, which, although less pathogenic than anticipated, may acquire additional virulence-associated mutations in the future. To estimate the potential risk, we sequentially passaged the isolate A/Hamburg/04/2009 in A549 human lung epithelial cells. After passage 6, we observed a 100-fold increased replication rate. High-throughput sequencing of viral gene segments identified five dominant mutations, whose contribution to the enhanced growth was analyzed by reverse genetics. The increased replication rate was pinpointed to two mutations within the hemagglutinin (HA) gene segment (HA_1 D130E, HA_2 I91L), near the receptor binding site and the stem domain. The adapted virus also replicated more efficiently in mice *in vivo*. Enhanced replication rate correlated with increased fusion pH of the HA protein and a decrease in receptor affinity. Our data might be relevant for surveillance of pre-pandemic strains and development of high titer cell culture strains for vaccine production.

Introduction

In 2009, there was a pandemic outbreak of a new H1N1 influenza A virus (IAV) originating in Mexico. The pandemic virus consisted of a unique combination of gene segments, that is not present in any other IAV isolate. Based on genetic sequence analyses, this pandemic virus was found to originate from multiple reassortments of avian, swine, and human viruses and probably circulated in the North American swine population for over a decade (Smith et al., 2009). The initial pandemic H1N1 2009 virus revealed no virulence markers, simply because the adaptation to the human system had not taken place (Garten et al., 2009). Therefore, it is expected that such adaptive mutations will occur and manifest in the human 2009-pandemic H1N1 lineage in the future. Indeed, several studies reported occurrence of such adaptive mutations (Pan et al., 2010; Otte et al., 2015; Jimenez-Alberto et al., 2013; Elderfield et al., 2014; de Vries et al., 2013).

The most efficient clinical countermeasure against the threat of impending pandemic IAV infections is vaccination. Classically, influenza vaccines have been produced in embryonated chicken eggs but several cell culture-based systems are also available, which possess certain advantages over egg-based production

* Corresponding author at: Department of Molecular Biology, Max Planck Institute for Infection Biology, Berlin, Germany
E-mail addresses: meyer@mpiib-berlin.mpg.de (T.F. Meyer), karlas@mpiib-berlin.mpg.de (A. Karlas).
[1] These authors contributed equally to this work.
[2] Present address: Laboratory of Experimental Biophysics, École Polytechnique Fédérale de Lausanne (EPFL), Lausanne, Switzerland.
[3] Present address: Bacterial Vaccines Discovery and Early Development, Janssen Pharmaceuticals (Johnson & Johnson), Bioscience Park Leiden Zernikedreef 9, 2333 CK Leiden, The Netherlands.

http://dx.doi.org/10.1016/j.virol.2016.02.002

systems, such as faster scalability (Genzel et al., 2006), potentially higher antigenicity (Katz and Webster, 1992), and lack of egg-derived allergens (James et al., 1998). Unfortunately, cell culture-based systems often provide lower titers than egg-based systems (Feng et al., 2011). Thus, there is also a strong need to optimize cell culture-based vaccine production.

In our hands, an early 2009-pandemic H1N1 virus isolated in Europe, A/Hamburg/04/2009 (HH/04), grew inefficiently in cell culture compared to lab-adapted strains such as A/WSN/1933 or A/Puerto Rico/08/1934. We serially passaged HH/04 in A549 cells, the standard cell culture model for IAV research, to identify determinants of adaptation to these cells. Indeed, after six passages we noticed an abrupt rise in the virus titer. Deep sequencing analysis and use of reverse genetics systems enabled us to pinpoint the improved virus replication down to two mutations in the HA gene segment. Importantly, the mutated virus not only replicated more efficiently in cell culture systems, but also in lungs of infected mice. Follow-up analyses revealed that these two mutations improve replication due to different receptor affinity and altered pH during HA-mediated fusion with the host cell membrane. Our findings are relevant to both influenza surveillance and cell culture-based vaccine production.

Materials and methods

Cell lines

All cell lines were cultivated at 37 °C and 5% CO_2. Madin Darby Canine Kidney (MDCK) cells (ATCC CCL-34) were grown in Dulbeccos's Modified Eagle Medium (DMEM, Invitrogen) supplemented with 10% fetal calf serum (FCS, Biochrome), 2 mM L-glutamine and 100 U/ml penicillin–streptomycin (P/S). Human alveolar basal epithelial cells (A549, ATCC CCL-185) and human embryonic kidney (HEK-293T) cells (ATCC CRL-11268) were grown in DMEM supplemented with 10% FCS, 2 mM L-glutamine, 1 mM sodium pyruvate and 100 U/ml P/S. Mouse lung epithelial (MLE-12) cells (ATCC CRL-2110) were grown in DMEM/F-12 supplemented with 2% FCS, 5 μg/ml insulin, 50 nM hydrocortisone and 100 U/ml P/S. Chinese hamster ovary (CHO) cells (ATCC CCL-61) were grown in DMEM supplemented with 10% FCS, 2 mM L-glutamine and 100 U/ml P/S. For transfection experiments medium was used without P/S.

Virus strains

Influenza virus strain A/WSN/33 (H1N1) was propagated in 11-day old embryonated chicken eggs for 2 days. The allantoic fluid was harvested and subjected to plaque assay and indirect immunofluorescence microscopy (IIFM) to quantify viral titer. The influenza wild type virus strain A/Hamburg/04/2009 (H1N1) (HH/04) was provided by Stephan Becker (University Marburg, Germany) and propagated in MDCK cells as described previously (Karlas et al., 2010). The A549-adapted variant HH/04-P6 was derived by serial passaging of HH/04 in A549 cells. To this end, A549 cells were initially infected with an MOI of 0.1 of the wild type virus, and 25% of the culture volume was transferred onto new A549 cells, each, after 2–6 days. Concentration of virus in the supernatants was quantified by plaque assay.

Next generation sequencing

Isolation of viral RNA from HH/04 P6 was done using Trizol LS (Life Technologies) following the standard protocol as described below. To remove DNA residues the Ambion DNA Treatment & Removal DNA-free Kit (Life Technologies) was used. The isolated viral RNA was then sent to the Max Planck Genome Centre Cologne where the genome of the mutated virus was sequenced on the Illumina HiSeq2000. The raw data was then subjected to different bioinformatical analyses. The initial quality control of the raw sequencing reads was performed using 'FastQC' (http://www.bioinformatics.babraham.ac.uk/projects/fastqc/). No significant problems with the data were revealed. Short reads were then aligned to the influenza HH/04 reference sequence (Genbank IDs: GQ166207, GQ166209, GQ166211, GQ166213, GQ166215, GQ166217, GQ166219, GQ166221) using 'Bowtie2' (Langmead and Salzberg, 2012). The resulting alignment was then analyzed by the tool 'Qualimap' in order to evaluate the mapping quality (Garcia-Alcalde et al., 2012). Qualimap reported a high duplication rate, which is expected due to extremely high coverage (around 50,000x per sequencing lane). To fix this problem, the alignment was refined using the 'GATK toolkit' (McKenna et al., 2010). Duplicates were removed and quality values were recalculated. The 'FreeBayes' software (Garrison E, 2012) was applied to discover the SNPs and short indels. The mutation rates for H1N1 virus variations were computed using Needle alignment tool (Rice et al., 2000).

Cloning of the recombinant influenza plasmids

Infectious culture supernatant from MDCK cells containing HH/04 wt and HH/04 P6 were used for isolation of viral RNA from virus particles. RNA was isolated using Trizol LS following the standard protocol. To remove DNA residues, the Ambion DNA Treatment & Removal DNA-free Kit (Life Technologies) was used. The isolated viral genome was translated into cDNA using RevertAid Premium First Strand cDNA Synthesis Kit (Thermo Scientific) according to the manufacturer's protocol, using the Uni12 primer (5'-AGCAAAAGCAGG-3') and 100 ng viral RNA. For cloning of recombinant influenza virus plasmids, gene segment specific primers were used to amplify the specific gene segments as previously described (Hoffmann et al., 2001). The PCR products amplified with the Pfu Turbo DNA-polymerase (Agilent) were purified and cloned into the recipient plasmid pHW2000 (Hoffmann et al., 2001) using the restriction enzyme BsmBI (Fermentas) according to the manufacturer's protocol. Due to the presence of the BsmBI and BsaI recognition sites within the polymerase acidic protein (PA) and nucleoprotein (NP) gene segments, the cloning strategy had to be modified and blunt ended PA and NP PCR products treated with the T4 polynucleotide kinase (Fermentas) were ligated with the pHW2000 plasmid, which was previously digested with BsmBI and treated with the T4 DNA Polymerase (NEB) to achieve compatible blunt ends. After successful cloning, all plasmids were sequenced by Sanger sequencing.

Site-directed mutagenesis

To be able to characterize each individual mutation within the HA gene segment separately, the HA plasmid sequence was mutated using the Quick change II Site-Directed Mutagenesis Kit (Stratagene) according to manufacturer's protocol. The following oligonucleotides were used: HA-a464c: 5'-CAAGTTCATGGCCCAATCATGACTCGAACAAAGGTGTAA-3'; HA-a464c_as: 5'-TTACACCTTTGTTCGAGTCATGATTGGGCCATGAACTTG-3'; HA-c1335a: 5'-GATGATGGTTTCCTGGACATTTGGACTTACAATGCCG-3'; HA-c1335a_as: 5'-CGGCATTGTAAGTCCAAATGTCCAGGAAACCATCATC-3'. All plasmids were verified by Sanger sequencing.

Generation of recombinant viruses

For transfections, HEK-293T cells were cultured in tissue culture flasks with the appropriate medium (see above). After 24 h

confluent cells were transfected with eight different plasmids encoding the eight different influenza gene segments by using Lipofectamine® LTX & Plus Reagent (Life Technologies) according to manufacturer's protocol. To increase the amount of virus particles MDCK cells were added 6 h post-transfection (p.t.) to the transfected HEK-293T cells. After 24 h at 37 °C and 5% CO_2 HEK-293T and MDCK cells were washed with DPBS (Invitrogen) and medium was replaced with infection medium (standard culture medium with replacement of FCS with 0.2% BSA) containing TPCK-treated trypsin (1 μg/ml). Subsequently, the cells were incubated at 37 °C for an additional 48 or 72 h. To determine the virus titer, supernatants were titrated onto MDCK cells by standard plaque assay using agarose overlay medium.

Infection-growth kinetics

A549 cells or MLE-12 cells were infected with the indicated recombinant viruses for growth kinetics. 50,000 cells were cultured in the appropriate medium in 6-well plates the day before. The medium was removed and cells washed with DPBS. Virus was diluted into infection buffer containing DPBS, 0.2% BSA, $CaCl_2$ (492 μM) and $MgCl_2$ (901 μM) to achieve the indicated MOI, and 500 μl transferred onto cells and incubated at RT for 1 h. Medium was then replaced with 2 ml infection medium (standard culture medium with 0.2% BSA instead of FCS) containing TPCK-treated trypsin (1 μg/ml). Infected cells were incubated at 37 °C and 5% CO_2 for 48 or 72 h. At indicated time points 600 μl of supernatant was harvested and replaced by fresh infection medium. The supernatants were centrifuged for 10 min at 1500*g* and 4 °C and transferred to MDCK cells to determine viral titers by standard plaque assay.

Animal experiments

Animals were housed and bred under pathogen-free conditions in biosafety level 2, according to the German Animal Protection Law (Tierschutzgesetz TierSchG). The animal experiments were approved by the local authorities (Landesamt für Gesundheit und Soziales Berlin LAGeSo: Reference number G0096/14). BALB/c mice were provided by Charles River (Sulzfeld, Germany). Mice aged between 7 and 15 weeks were intranasally infected with the recombinant HH/04 wt influenza virus and its derivates (5.0×10^4 PFU in 50 μl). Two days later, animals were euthanized and their lungs isolated and homogenized, followed by centrifugation at 800*g* for 8 min at 4 °C. The amount of infectious viruses in the supernatant was quantified using the standard plaque assay.

Fusion assay

CHO cells were transfected with the individual HA plasmid using TurboFect (Thermo Scientific). Concentrate of human erythrocytes in additive solution was provided by the local blood bank (DRK-ITM Berlin, Germany). Red blood cells (RBCs) were washed three times with PBS at 4 °C. To check the ability of the HA mutants to fuse with membranes at different pH levels, RBCs were stained with calcein AM (Sigma) and octadecyl rhodamine B chloride (R18, Thermo Scientific) as described previously (Morris et al., 1989; Mair et al., 2014). For activation of the HA the transfected CHO cells were incubated in PBS containing 0.5 U neuraminidase (neuraminidase from *Clostridium perfringens* (*C. welchii*, Sigma-Aldrich) and 4 μg/ml TPCK-trypsin on ice for 5 min followed by addition of serum containing medium. Subsequently, the stained RBCs were added to transfected CHO cells and incubated at RT for 1 h while gently shaking. After washing with PBS every sample was imaged to exclude pH-independent fusion. Subsequently, samples were incubated with the fusion buffer containing 10 mM 2-[4-(2-Hydroxyethyl)-1-piperarzine)-1-yl] ethanesulfonic acid (HEPES), 10 mM 2-(*N*-Morpholino)ethanesulfonic acid and 100 mM sodium chloride in water to start the fusion process. The fusion buffer remained on the cells for an incubation of 5 min at 37 °C. Afterwards, the buffer was replaced with PBS at neutral pH and the sample stored for 2–5 min at 37 °C. Finally, the sample was imaged under a confocal microscope (Olympus FluoView FV 1000), the cells were identified manually and the mean calcein intensities for the regions of interest (ROI) were calculated and normalized based on the minimal and maximal intensities.

Single-virus force spectroscopy (SVFS)

AFM tip chemistry

Commercially available AFM cantilevers (MSCT, Bruker) were amine functionalized by using the room-temperature method for reaction with APTES (Rankl et al., 2008). A heterobifunctional PEG linker, acetal–PEG_{800}–NHS (N-hydroxysuccinimide), was attached by incubating the tip for 1.5–2 h in 0.5 ml of chloroform containing 2 mg/ml acetal–PEG–NHS and 8 μl triethylamine, resulting in acylation of surface-linked APTES by the NHS group (Wildling et al., 2011). The terminal acetal group was converted into an amine-reactive aldehyde by incubation in 1% citric acid as described previously (Rankl et al., 2008). After rinsing three times with water, once with ethanol and drying under a stream of nitrogen, the tips were incubated in a mixture of 19–25 μl of approximately 0.6–1.6 mg/ml influenza A virus in PBS (without Ca^{++}) and 1–2 μl of 1 M $NaCNBH_3$ (freshly prepared by dissolving 32 mg of solid $NaCNBH_3$ in 500 μl of 10 mM NaOH) for 60 min. The tips were then washed in 3 ml PBS for 3 times and stored in PBS at 4 °C. All other chemicals and reagents were purchased from different commercial sources in the highest purity grade available.

SVFS measurement

AFM-based force spectroscopy was performed with an Agilent 5500 AFM. The Petri dish with cells was mounted with the AFM, which was put on the optical microscope through a specially designed XY stage. Before force measurements, the cantilever with a nominal spring constant of 10 pN/m functionalized with influenza A virus was incubated in 5 mg/ml BSA for 30 min in order to minimize the nonspecific interaction between the cantilever tip and the cell surface. Measurements were performed in PBS buffer at room temperature. After the cantilever tip approached to the cell surface, force distance curves were repeatedly measured with Z-scanning range of 2 μm, cycle duration of 0.5–8 s, 500 data points per curve, and typical force limit of about 40–70 pN. The spring constants of the cantilevers were determined by using the thermal noise method (Hinterdorfer et al., 1996).

Fitting of SVFS data

Similar to single molecule force spectroscopy (SMFS), also in SVFS studies, several hundred force distance cycles are recorded in a dynamic range of increasing loading rates under identical conditions. For each of these force curves showing unbinding events, the unbinding force *Fi* and the effective spring constant k_{eff} (slope at rupture) were determined. The loading rates *r* were determined by multiplying the pulling velocity *v* with the effective spring constant k_{eff} (*i.e.* $r = v * k_{eff}$). Additionally, a rupture force probability density function (pdf) was calculated and a Gaussian distribution was fitted to the main peak of the pdf. Subsequently, all unbinding events within $\mu \pm \sigma$ of the fit have been selected to create a loading rate dependence scatter plot for further

calculations of k_{off} and x_u. Generally, the loading rate r is constant for a fixed pulling speed, which implies, that the effective spring constant k_{eff} does not vary significantly. However, for force spectroscopy measurements on living cells it is known that k_{eff} could show a broadened distribution caused by local variations of the spring constant of the cell surface, leading to a convolution of the rupture force distribution and further influences the calculations for the dissociation rate constant, k_{off}, and the separation of the receptor-bound state to the energy barrier, x_u. To circumvent this influence, we applied a maximum likelihood routine to fit the SVFS data to the Evans-model (Wildling et al., 2012), in order to obtain k_{off} and x_u.

According to the single energy barrier binding model, the probability p that the complex breaks at a certain force, F, is given as (Evans and Ritchie, 1997):

$$p(F) = \frac{k_{off}}{rk_BT}\exp\left[\frac{Fx_u}{k_BT} - \frac{k_{off}}{rx_u}\left(exp\frac{Fx_u}{k_BT} - 1\right)\right] \quad (1)$$

The parameters x_u and k_{off} were determined by applying a maximum likelihood approach, in which the negative log likelihood *nll* was minimized by modifying k_{off} and x_u, with p based on Eq. (1) defined in the single barrier model (Evans and Ritchie, 1997):

$$nll = -\sum_t \log p(k_{off}, x_u, F_t, r_t) \quad (2)$$

Binding assay

Equal copy numbers of recombinant HH/04 wt and HH/04 HA_1 D130E + HA_2 I91L viruses were either directly lysed with Trizol LS (input control) or incubated at 4 °C for 1 h together with A549 cells seeded the day before. Subsequently, the cells were lysed with Trizol LS and the RNAs of the input control and the infected cells were isolated. To be able to adjust different RNA yields during the RNA isolation, the input controls and the cell lysates were spiked with a defined amount of lentiviral particles encoding the enhanced green fluorescent protein (EGFP). The amount of applied (input control) and attached viruses was determined by quantitative RT-PCR using NP specific oligonucleotides (NP_for: 5'-CCACAAGAGGGGTCCAGATT-3', NP_rev: 5'- GCACTGAGAATGTAGGCTGC-3') in consideration of the amount of isolated RNA quantified by EGFP specific oligonucleotides (EGFP_for: 5'-ACGTAAACGGCCACAAGTTC-3', EGFP_rev: 5'- AAGTCGTGCTGCTTCATGTG-3').

Electron microscopy

Cells were seeded into an ibidi μ-slide 18 well (ibidi GmbH, Planegg, Martinsried), infected with recombinant HH/04 wt and HH/04 HA_1 D130E + HA_2 I91L viruses (MOI 7) and fixed at 16 h p.i. with 2.5% glutardialdehyde. Cells were post-fixed with osmiumtetroxide, contrasted with tannic acid and dehydrated using an ascending ethanol series. After critical point drying, the specimen was coated with 3 nm platinum/carbon and analyzed in a Leo 1550 field emission scanning EM.

Glycan array

Glycan array preparation was performed as described previously (Pereira et al., 2015). Briefly, glycans containing a primary amino linker were dissolved at a concentration of 0.1 mM in printing buffer (50 mM sodium phosphate, pH 8.5) and printed on N-hydroxysuccinimide activated glass slides (CodeLink slides, Surmodics, Edina, MN, USA) using an S3 robotic microarray spotter (Scienion, Berlin, Germany). Slides were incubated overnight in a humidity saturated chamber and remaining reactive groups were quenched by incubating with 100 mM ethanolamine, 50 mM sodium phosphate at pH 9.0 for 1 h at room temperature. Slides were washed with water, dried by centrifugation and stored at 4 °C until use. Before loading, the array was washed with DPBS. Virus was diluted as indicated into sterile binding buffer containing 1% BSA, 0.05% Tween 20 (MERCK), $CaCl_2$ (492 μM) and $MgCl_2$ (901 μM) at pH 7.0. 30 μl of diluted virus was pipetted in each well and the array was incubated in a moist chamber for 24 h at 4 °C. Each well was then washed three times with washing buffer containing DPBS and 0.1% Tween 20 (DPBS-T). Subsequently, wells were blocked with DPBS containing 1% BSA for 2 h at 4 °C and permeabilized using DPBS-T containing 0.3% Triton-X100. To stain the bound virus the array was incubated with a primary monoclonal antibody against the viral NP protein (1:1000, clone AA5H, AbD Serotec, Oxford, UK) at 4 °C overnight. Primary antibody was removed and wells were washed three times with DPBS-T. Secondary Cy3-coupled goat anti-mouse IgG (1:100, product-code: 115-165-146, Jackson ImmunoResearch Laboratories, West Grove, PA, USA) was added and incubated at RT for 1 h. The array was washed three times with DPBS-T and dipped into distilled water before scanning. Glycan array fluorescence images were obtained using a GenePix 4300A microarray scanner (Molecular Devices, Sunnyvale, CA, USA). Fluorescence intensities of spots were evaluated with GenePix Pro 7.2 (Molecular Devices).

Results

Adaption of the H1N1 virus to human cells

To investigate the potential of HH/04 wt to adapt to human cells, we serially passaged the virus in A549 human lung epithelial cells and recorded the virus titer in the supernatants starting at passage 4 (Fig. 1A). We observed a sudden increase of the titer after passage 6 (Fig. 1B). Interestingly, both HH/04 wt and HH/04 P6 (and the lab adapted strain A/WSN/1933) infect A549 cells with similar efficiencies, however, HH/04 P6 grows to 10- to 100-fold higher virus titers compared to HH/04 wt in A549 cells (Fig. 1C and D).

Next generation sequencing identification of mutations acquired by HH/04 P6

To detect mutations in the genome of the adapted H1N1 virus (HH/04 P6) that lead to the improved replication rates in A549 cells, the genome of the mutant was subjected to next generation sequencing. To this end, RNA from these viruses was isolated and sequenced using the Illumina platform. Due to the small genome of influenza viruses, all gene segments could be sequenced with a high coverage thereby increasing the precision of sequence analysis and enabling detection of mutations that are only present in a small percentage of the virus genome. To exclude false positive mutations, which might potentially result from technical difficulties during the sequencing procedure, we focused on mutations with a frequency of more than 20%. All mutations identified by this procedure are shown in Fig. 2A. Interestingly, the processed data illustrate that some gene segments like the HA gene show higher variability than others. Cleavage of the HA full length protein (HA_0) by cellular proteases leading to HA_1 and HA_2 is required to allow fusion with the host cell membrane and therefore represents an essential step during IAV replication (Peitsch et al., 2014; Klenk et al., 1975; Steinhauer, 1999). Remarkably, we identified a total of 5 mutations with a frequency of more than 20% located in both HA_1 and HA_2.

After examining the different mutations on the RNA level, we analyzed whether they also have an impact on the amino acid

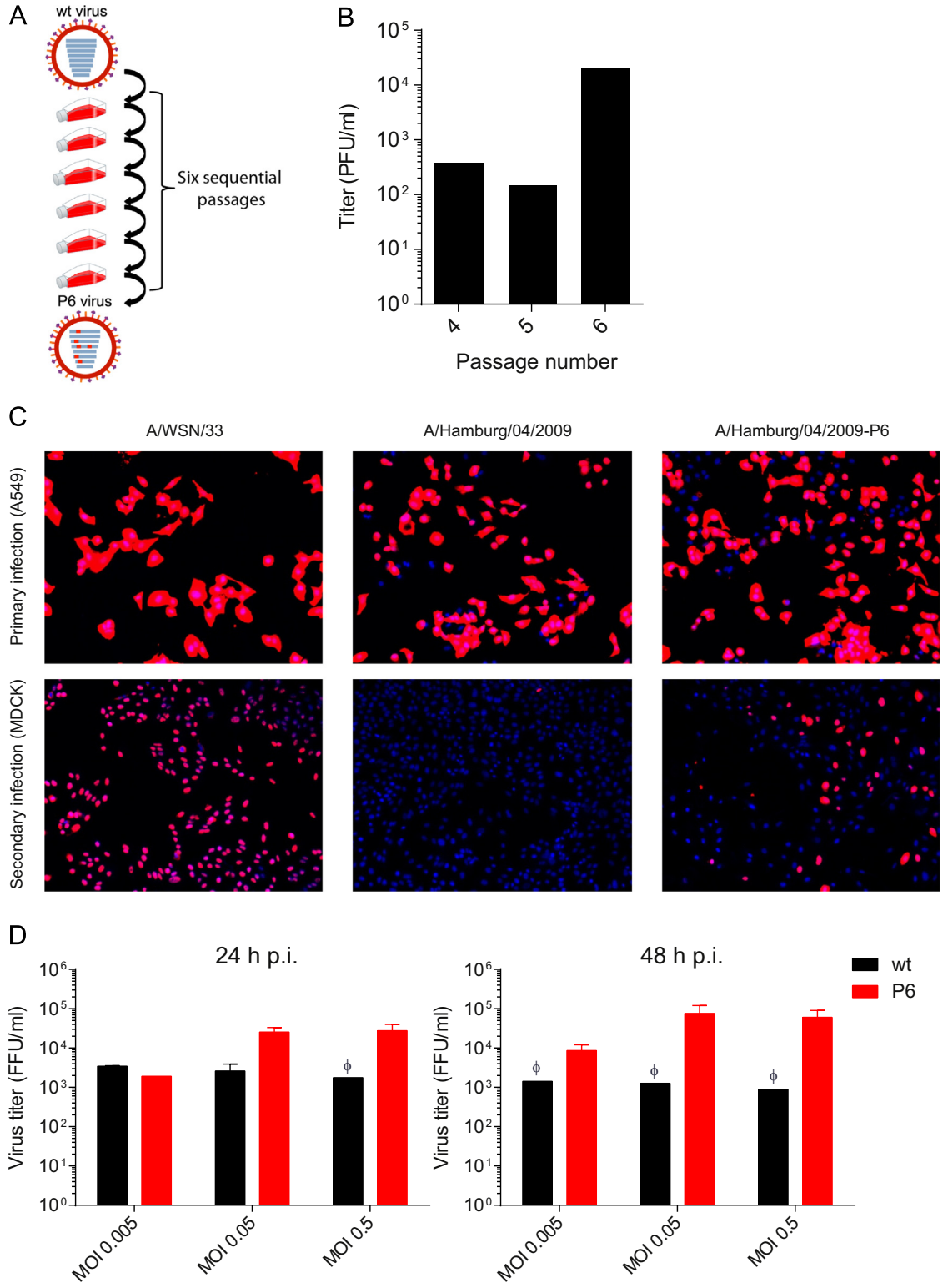

Fig. 1. Adaptation of A/Hamburg/04/2009 (wt) to A549 cells and infection characteristics of the adapted virus. (A) HH/04 was serially passaged six times in A549 cells to generate the HH/04 P6 virus. (B) Virus titers in supernatants generated as depicted in (A) were determined by plaque assay from passage 4, onwards. After passage 6, no further increase in virus titer was observed. (C) Representative indirect immunofluorescence microscopy (IIFM) images to compare the virus infection rates of wt and P6 viruses. A549 cells were infected at MOI 0.5 with A/WSN/1933, HH/04 wt and HH/04 P6 viruses for 24 h in TPCK-trypsin-free medium (upper panel). At 48 h p.i. supernatants were transferred onto MDCK cells for 7 h in TPCK-trypsin containing medium (lower panel), before labeling DNA (blue) and viral nucleoprotein (red). (D) A549 cells were cultivated for 48 h and, infected with HH/04 wt and HH/04 P6 at indicated MOIs. At 24 or 48 h, culture supernatants were transferred to MDCK cells to quantify virus titer *via* FFA. The HH/04 P6 virus exhibits a 10- to 100- fold higher virus titer compared to wt in A549 cells. Results represent the mean+SD for the technical replicates of one experiment. *Φ*: no SD was determined.

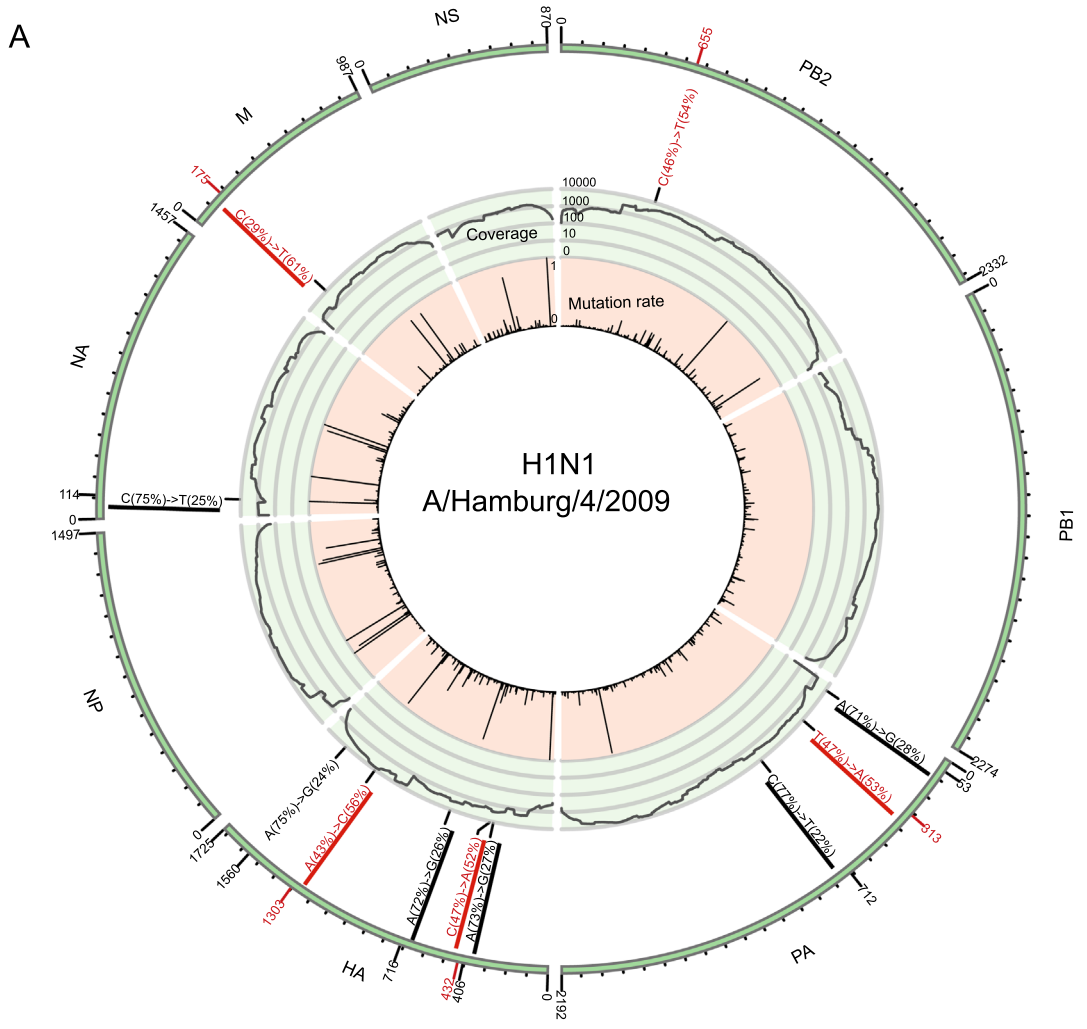

B

Mutation on protein (RNA) level	Pandemic human IAVs from 04/01/2009 until 09/03/2015			Human IAVs			All IAVs		
	No. of sequences	wt (%)	P6 (%)	No. of sequences	wt (%)	P6 (%)	No. of sequences	wt (%)	P6 (%)
PA F105I (313nt T→A)	5265	99.72	0	12535	99.47	0	29520	98.52	0
HA1 D130E (432nt C→A)	5180	99.50	0.39	23118	48.80	0.27	45518	30.32	3.00
HA2 I91L (1303nt A→C)	5180	99.98	0	23118	49.97	0.02	45518	30.60	0.60
NA T32I (114nt C→T)	8832	0.07	99.89	20538	42.90	56.39	41760	42.08	39.70
M P54S (175nt C→T)	6900	99.96	0.04	18033	99.97	0.03	40193	99.47	0.48

C

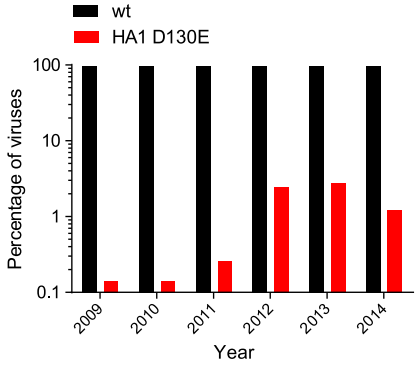

Fig. 2. Overview of identified mutations in the gene segments of the HH/04 P6 genome. The analysis of mutations in different gene segments detected by Next Generation Sequencing was performed using the software package Unipro UGENE (Okonechnikov et al., 2012). (A) The Circos plot (Krzywinski et al., 2009) shows (i) coverage rate of Illumina sequencing reads (green background) (ii) the genetic variability of each gene segment based on all available human p2009 H1N1 viruses (NIAID Influenza Genome Sequencing Project) (red background) and (iii) mutations on RNA level based on the available A/Hamburg/04/2009 virus sequence information (Genbank IDs: GQ166207, GQ166209, GQ166211, GQ166213, GQ166215, GQ166217, GQ166219, GQ166221). Mutations represented in $>20\%$ or $>50\%$ of the specific gene segment are depictured in black and red, respectively. Mutations leading to a change in the amino acid sequence of the coded protein are underlined. (B) Frequency of identified mutations in (i) human pandemic H1N1 viruses isolated from patients between 2009 and 2015, (ii) human IAVs and (iii) all IAVs isolated from various species. (C) Frequency of HA_1 D130E mutation in human pandemic H1N1 viruses isolated from patients between 2009 and 2014.

sequence of the corresponding viral proteins. Furthermore, we assumed that mutations leading to significantly enhanced virus replication manifest in the viral quasispecies after several passages. Thus, we focused on mutations that occur at a frequency of more than 50%. Interestingly, nearly all mutations that are present with a frequency above 20% in the mutant virus quasispecies lead to an amino acid change with exception of the mutation in PB2 at position 655 bp and in HA at position 1560 bp.

Next, we compared the amino acid sequence of the HH/04 wt and the adapted HH/04 P6 viruses to sequences of (i) other 2009-

pandemic H1N1, (ii) all human influenza A (including *e.g.* H3N2) and (iii) all influenza A viruses derived from any host species, based on the dataset provided by the NIAID Influenza Genome Sequencing Project (http://www.ncbi.nlm.nih.gov/genomes/FLU/FLU.html). In general, this comparison revealed that some of the detected mutations are present in other H1N1 pandemic viruses from 2009 to 2015 (Fig. 2B). However, the mutations detected by us are in general underrepresented in comparison to all published sequences, with the exception of one mutation in the NA gene segment (NA T32I) which is present in nearly all pandemic 2009 H1N1 viruses. Remarkably, the mutation HA_1 D130E is only rarely present in pandemic H1N1 viruses in the years 2009 and 2010 (0.14%, each), but significantly increases during subsequent years to up to 2.80% (Fig. 2C). The mutation HA_2 I91L, however, could only be found within a few swine IAVs and a single human influenza virus from 2006 (A/Gholestan/215/2006).

In vitro analysis of reverse genetics chimeras of HH/04 wt and HH/04 P6

To identify those mutations that contribute the most to the improved replication rate of the adapted virus, we used a reverse genetics system to clone all influenza gene segments of the HH/04 wt and HH/04 P6 virus (Hoffmann et al., 2001). Here, we focused on the four most abundant mutations that cause a change of the amino acid sequence of the HH/04 P6 virus and one mutation within NA which was highly frequent in pandemic-2009 H1N1 viruses (Fig. 2B). To be able to test every single gene segment separately, we combined the individual gene segments with seven plasmids encoding gene segments of the influenza virus strain A/WSN/1933 and analyzed replication of the chimeras, as described previously (Hoffmann et al., 2000). All generated plasmids led to production of infectious viruses, but with notable variation (Supplementary Fig. S1). Interestingly, the chimera containing the HA segment of HH/04 wt displayed a strongly reduced virus titer compared to the adapted counterpart. Based on these initial experiments, we confirmed that all generated plasmids are capable of producing replication-competent viruses. To identify which of the mutations are causative to the enhancement of virus growth, recombinant viruses were produced and replication rates recorded for 72 h (Fig. 3A). As expected, the HH/04 P6 virus (containing all five mutations) replicated to the highest titers, whereas the wild type virus showed a two-log lower final titer. The wild type virus containing only the two mutations in the HA segment (HA_1 D130E+HA_2 I91L, Supplementary Fig. S2) showed similar growth characteristics as HH/04 P6, and both mutations contribute to this effect. In contrast, none of the other three mutations led to a significant improvement of virus replication.

Characterization of the recombinant viruses in vivo

Although HH/04 had been adapted to human A549 cells, we tested whether the mutations HA_1 D130E and HA_2 I91L also enhance virus replication in other species, using the mouse as a model. First, we examined viral replication in MLE 12 murine lung epithelial cells. Indeed, both mutations, either separately or in combination, led to enhanced replication (Fig. 3B). Subsequently, we infected mice either with the HH/04 wt, the single mutants (HA_1 D130E, HA_2 I91L) or the double mutant (HA_1 D130E+HA_2 I91L). To ensure comparability, 7.3×10^3 PFU, *i.e.* the maximum titer achieved for the virus that replicated least efficiently (HH/04), was applied for all virus variants intranasally in a volume of 30 µl and lungs harvested already 48 h later, to prevent loss of animals due to adverse effects associated with the infection. Indeed, those viruses that harbor either one or both mutations led to a significantly increased virus titer in the murine lung compared to the wt virus (Fig. 3C). The mutation HA_1 D130E seemed to be more important, leading to higher titers than mutation HA_2 I91L. Future experiments will show if the survival rate of those animals

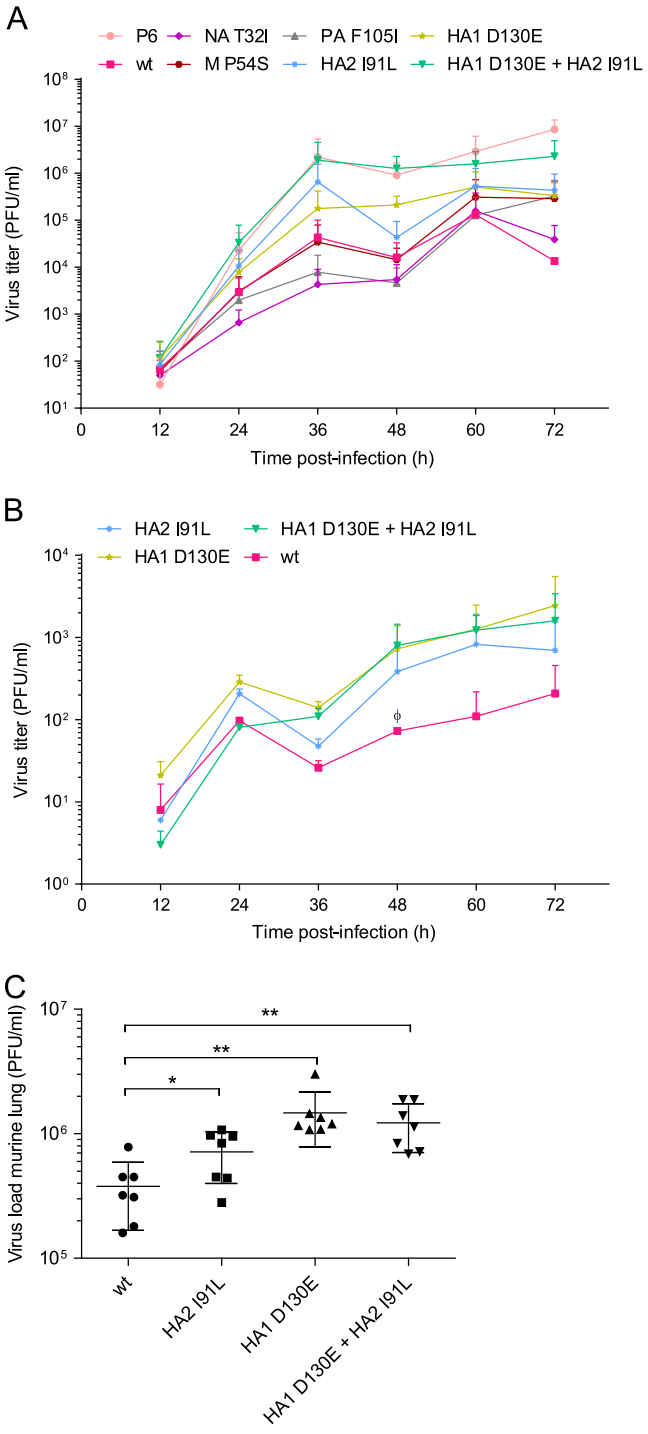

Fig. 3. Characterization of the newly generated recombinant viruses by reverse genetics. (A and B) Growth curves of recombinant viruses in two different cell lines. A549 cells (A) or MLE-12 cells (B) were infected at MOI 0.01 with indicated recombinant viruses for 72 h in TPCK-trypsin-containing medium. At the indicated time points culture supernatant was transferred to MDCK cells to quantify virus titer *via* plaque assay. The results represent the mean+SD for two experiments. ϕ: no SD was determined. (C) Seven mice were intranasally inoculated with 30 µl containing 7.3×10^3 PFU of each indicated recombinant virus for 48 h. Mouse lungs were isolated, homogenized and viral loads quantified *via* plaque assay. The results represent the mean ± SD. Statistical analysis was performed by unpaired *t*-test: $^{*}p < 0.05$, $^{**}p < 0.01$.

infected with the adapted virus is also reduced compared to those infected with the wild type virus.

Comparison of the structure of the HA surface protein of HH/04 wt and HH/04 P6

Based on the crystal structure of a reference pandemic H1N1 2009 isolate (Xu et al., 2012), we were able to determine the position of HA_1 D130E and HA_2 I91L in the HA trimer. Interestingly, HA_1 D130E is located within the globular head domain of the HA_1 subunit, a position potentially relevant to the receptor specificity (Fig. 4A and B). HA_2 I91L, on the other hand, is located in the long α-helix of the HA stem and may influence the stability of the HA trimer and could therefore lead to altered fusion properties (Fig. 4A–C). As expected, both mutations changed neither virion morphology (Fig. 4D and E) nor the ratio of spherical to filamentous particles (data not shown), as indicated by electron microscopy.

Functional analysis of HA_1 D130E and HA_2 I91L

To investigate whether mutations HA_1 D130E and HA_2I91L exhibit altered receptor specificity, we analyzed both virus strains using glycan arrays containing 15 different glycans typically found in mammalian cells. Unexpectedly, we did not detect significantly different binding profiles to the individual SAs between any of the virions tested (Supplementary Fig. S3), neither in the binding prevalence for α2,3Gal- or α2,6Gal-linked SAs, nor in the overall binding capacity to SAs. The highest affinity among all viruses we tested was observed for sialyl-Lewis^X (Neu5Acα2,3Galβ1,4 (Fucα1,3)GlcNAc-R), which is highly abundant on mammalian cells (Vainer et al., 1998).

While glycan arrays are an excellent tool for screening large numbers of structurally different receptors, they deviate greatly from a living cell surface. The local concentration and orientation of sialylated receptors are not well controllable and have been shown to influence virus binding (Papp et al., 2011). Single-virus force spectroscopy (SVFS) allows measuring virus-cell specificity at the level of individual viruses on living cells, *i.e.* conditions that mimic the natural situation very closely (Herrmann and Sieben, 2015). Here we used atomic force microscopy (AFM)-based SVFS (Supplementary Fig. S4). Briefly, AFM cantilevers are functionalized with purified influenza A viruses using specific attachment protocols (Rankl et al., 2008; Sieben et al., 2012). After lowering the cantilever onto a suitable living cell until touching the cell surface (Supplementary Fig. S4B and C), the cantilever is retracted, while interaction forces are detected with single-molecule resolution. Force–distance cycles are then recorded at various pulling speeds to infer the dissociation rate k_{off}, a parameter that can be used to compare the strength of cell binding between different virus strains (Sieben et al., 2012). To investigate whether mutations HA_1 D130E and HA_2 I91L exhibit altered cell binding characteristics, we compared the binding of HH/04 wt and HH/04 P6 to human A549 cells (α2,6-linked SAs > α2,3-linked SAs) and Chinese Hamster Ovary (CHO) cells (α2,3-linked SAs only (Takeuchi et al., 1988) (Supplementary Fig. S5). Since CHO cells do not express α2,3-linked SAs (Xu et al., 2011), we used this cell line in comparison to A549 to be able to identify differences in cell specificity. As evident from the elevated dissociation rates (Fig. 4F), the mutated virus (HA_1 D130E + HA_2 I91L) bound more weakly to both cell types than HH/04 wt. While the effect on CHO binding was not particularly strong (1.5 fold increased k_{off}), the binding strength to A549 cells was reduced by ~8-fold.

To obtain further evidence, we incubated the different virus variants, including the viruses containing only a single mutation, with A549 cells at 4 °C and quantified the amount of bound virus by quantitative RT-PCR. In line with the SVFS data, nearly the entire inoculum (86%) of the wild type virus bound to the cells, while adherence of the mutant virus was significantly lower (20%) (Fig. 4G). The virus variants containing single mutations revealed a reduced binding capacity to A549 cells compared to the wild type virus. However, none of these viruses reached the low adherence level of the mutant virus (HA_1 D130E + HA_2I91L).

It has been shown previously that mutations in the HA stem loop influence the pH of HA-mediated membrane fusion (Galloway et al., 2013). Since the HA_2 I91L mutation is localized in this domain, we determined whether one or both of the acquired mutations in HA affect the pH at which fusion can occur. Indeed, the HA_2 I91L virus revealed a fusion pH increased by 0.2 units (Fig. 5A and B). In contrast, the mutation HA_1 D130E virus exhibited the same fusion pH as HH/04 wt. Interestingly, the double mutant showed an intermediate effect, indicating that HA_1 D130E counteracts the effect of HA_2 I91L.

Discussion

In the present study, we adapted a 2009-pandemic H1N1 IAV (HH/04) to growth in A549 cells by serial passaging, and analyzed the adaptive mutations by next-generation sequencing. Our insights surpass those gained using bulk Sanger sequencing or Sanger sequencing of individual plasmid clones. We observed four dominant non-synonymous mutations in the A549-adapted virus compared to the wild type strain. Surprisingly, only two adaptive mutations, both located in HA, mediated the enhanced growth.

The HA_2 I91L mutation increased the pH at which HA-mediated fusion with the host cell membrane can occur and presumably contributes-together with the HA_1 D130E mutation-to a reduced affinity for α2,6- and α2,3-linked SAs, as well as for A549 cells. Although it seems more logical that the mutation HA_1 D130E, which is located close to the receptor binding site, is solely responsible for differences in virus adherence, our data suggest, that both mutations contribute to the reduced binding capacity. SVFS unraveled weaker binding of the mutant virus to A549 cells (expressing both α2,6- and α2,3-linked SAs), while binding to CHO (only α2,3-linked SAs) was almost unchanged. This result suggests that viruses have adapted towards less affine binding, particularly to A549 cells, which correlates with enhanced growth. Interestingly, the glycan specificity, as tested with glycan array binding, remained conserved. It should also be noted that this effect is not NA-related, since we used viruses carrying only mutations in HA. Changes in SA affinity during an adaptation process have been reported previously. Decreasing as well as increasing affinities have been observed, depending on the virus and model system (Kaverin et al., 1998; Imai et al., 2012; Hughes et al., 2000; Herfst et al., 2012; Gen et al., 2013; Bantia et al., 1998). Such mutations are required to optimize the interplay for a given host/model of HA (which binds SAs) and NA (which cleaves SAs) (Wagner et al., 2002). Similarly, changes in HA stability have also been reported when adapting influenza A viruses to a different system (Narasaraju et al., 2009; Murakami et al., 2012; Lin et al., 1997; Keleta et al., 2008). The stability optimum for the HA trimer appears to depend on factors such as the environmental pH (*e.g.* airway epithelium *versus* cell culture) or the cell-type-specific endosomal pH kinetics (Mair et al., 2014). Nonetheless, it remains obscure why an isoleucine to leucine mutation results in reduced pH stability, and why the aspartic acid to glutamic acid mutation contributes to a reduced SA affinity. Typically, mutations of isoleucine to leucine and aspartic acid to glutamic acid are considered conservative mutations that do not affect structure and function of the protein. However, evidence has been provided that even conservative mutations could be of significant consequence for

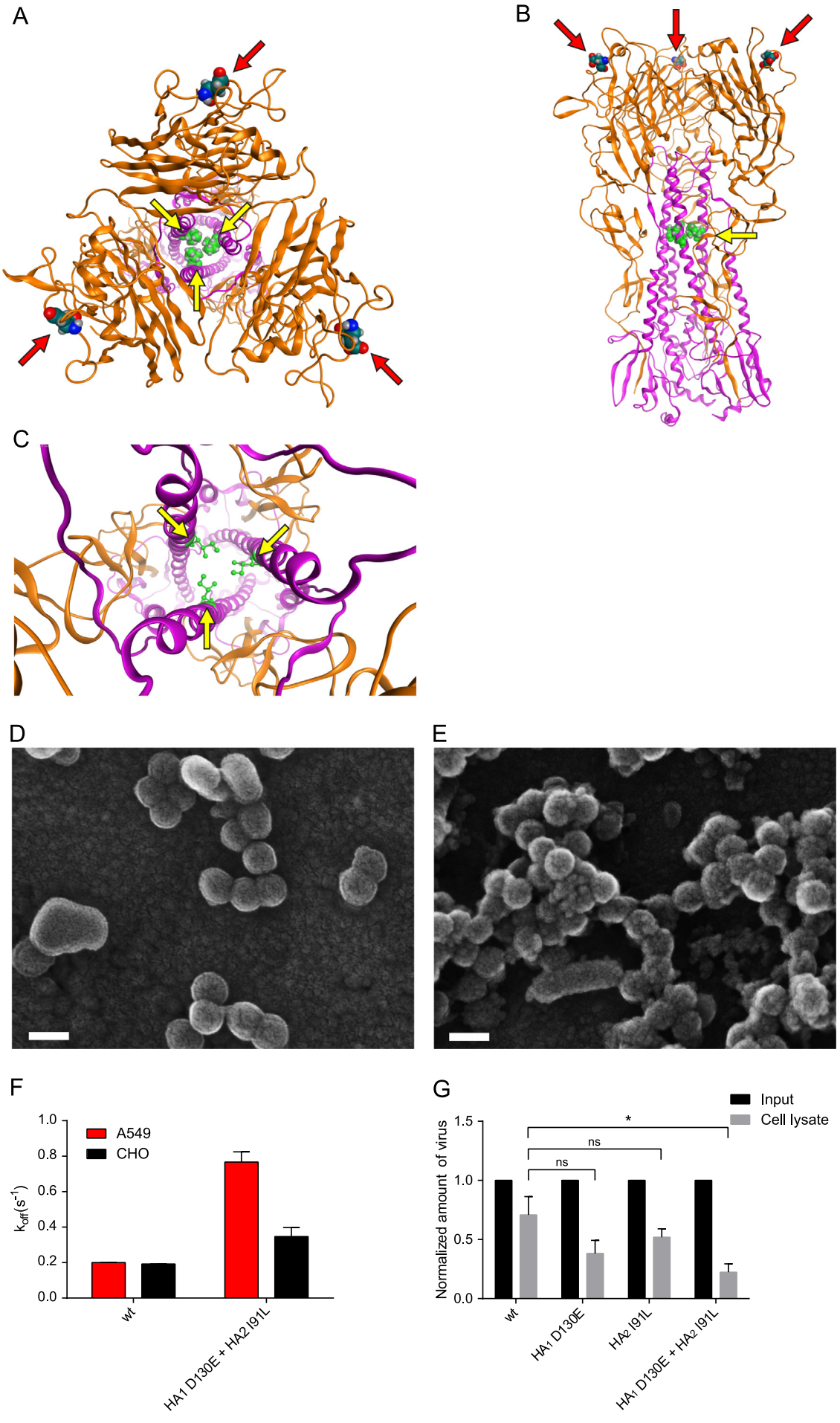
A
B
C
D
E
F
1.0
0.8
0.6
0.4
0.2
0.0
$k_{off}(s^{-1})$
A549
CHO
wt
HA1 D130E + HA2 I91L
G
Input
Cell lysate
Normalized amount of virus
1.5
1.0
0.5
0.0
*
ns
ns
wt
HA1 D130E
HA2 I91L
HA1 D130E + HA2 I91L

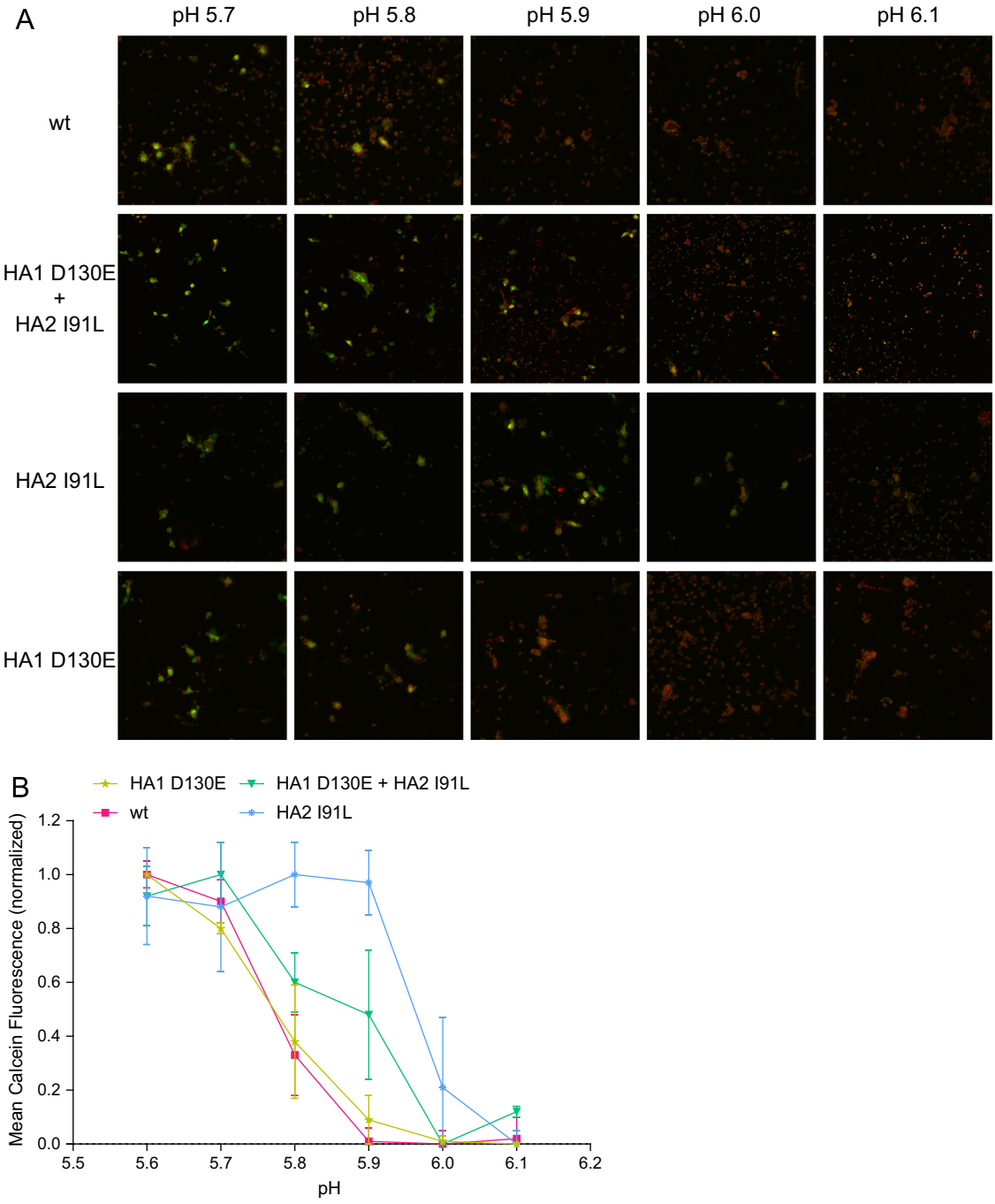

Fig. 5. pH-dependent membrane fusion properties of HA derived from wt and P6. CHO cells were transfected as indicated with plasmids containing the HA gene sequence of HH/04 wt, HA_1 D130E+HA_2 I91L or each mutation separately. 24 h after transfection the HA presented on the surface of CHO cells was activated using neuraminidase and TPCK-trypsin. RBCs stained with calcein (lumen) and R18 (membrane) were added and allowed to bind. After removal of unbound RBCs, membrane fusion with CHO cells was triggered by adding the fusion buffer at the indicated pH. (A) Representative images for indicated HAs at variable pH values. Transfer of calcein to CHO cells indicates successful cell–cell fusion. (B) Quantification of HA induced membrane fusion of red blood cells and CHO cells as depicted in A. The results represent the mean ± SEM for at least two experiments.

Fig. 4. Functional characterization of acquired mutations in HA gene segment. (A–C) Localization of the identified mutations within the hemagglutinin protein. Apical (A) and lateral (B) view of the HA trimer with the identified mutations in the stem loop (yellow arrows) and the receptor binding site (red arrows) (Gamblin et al., 2004; Sriwilaijaroen and Suzuki, 2012). (C) Apical view illustrating the position of the stem loop mutation (HA_2 I91L) in detail. The structure of HA was taken from the PDB database (PDB-ID 3UBE). (D+E) A549 cells were infected with HH/04 wt (D) or HH/04 HA_1 D130E+HA_2 I91L (E) at MOI 5 for 16 h, fixed and processed for electron microscopy. Scale bar=100 nm. (F) Live-cell binding characteristics of wt or HH/04 HA_1 D130E+HA_2 I91L to A549 and CHO cells as detected by SVFS. Influenza A virions were covalently attached to the AFM cantilevers using an acetal-PEG800-NHS crosslinker and force traces of virus-cell interactions were recorded at different pulling speeds (see Methods). Shown are the kinetic off-rate constants ($k_{off}(s^{-1})$), meaning that smaller values indicate stronger binding to the cells. (G) Binding capacity of wt, HA_1 D130E, HA_2 I91L or HH/04 HA_1 D130E+HA_2 I91L viruses to A549 cells. The amount of attached virus after 1 h incubation at 4 °C were quantified using quantitative RT-PCR normalized to the total amount of added virus (input). The results represent the mean ± SEM of at least three independent experiments. One-way Anova was used to calculate the significance of individual virus variants *versus* the wt virus ($^*p < 0.05$, ns $p \geq 0.05$).

structure and function of a protein. Recently, it was shown that isoleucine to leucine mutation causes a large change in conformation and temperature sensitivity of a DNA polymerase (Wu et al., 2015). Furthermore, very different spatial preferences for glutamic acid and aspartic acid have been reported (Jonson and Petersen, 2001).

The wildtype 2009-pandemic H1N1 IAV tested here appears to be well-suited for replication in A549 cells in tissue culture – apart from suboptimal receptor affinity and HA stability. These findings can be applied to the production of recombinant high-growth strains for vaccine production. However, antigenicity between a given parental strain and a high-growth strain with optimized receptor affinity and HA stability would have to be assessed. Furthermore, A549 cells are not approved as a vaccine production system, and the relevance of our findings for approved cell culture-based influenza vaccine production systems still needs to be demonstrated. In line with our results, decreased HA stability of influenza virus strain A/Puerto Rico/08/1934 was indeed correlated with increased replication efficiency in Vero cells, which is such a production line (Murakami et al., 2012).

Although we adapted HH/04 for growth in the human cell line A549, the two mutations in the HA gene segment also improved replication kinetics in murine cell culture and even in mice *in vivo*. Interestingly, a study comparing two A/Puerto Rico/08/1934 substrains, one replicating highly efficient and one replicating with low efficiency in mice, also identified differences in the HA gene. In line with our findings, the high growth strain showed decreased binding of α2,3-linked SAs and decreased trimer stability. However, in contrast to our observations, the highly efficient replicating strain also had an increased affinity to α2,6-linked sialic acids (Koerner et al., 2012). Our study emphasizes the role of receptor affinity and HA trimer stability, especially the two mutations in the HA segment identified here (HA_1 D130E, HA_2 I91L), as virulence factors of influenza viruses.

We also investigated the frequency of amino acids HA_1 E130 and HA_2 L91 in 2009-pandemic H1N1 viruses and all influenza A viruses from 2009 until 2014. While HA_2 L91 was not detected in the human population, the frequency of 2009-pandemic H1N1 isolates containing HA_1 E130 increased approximately 10-fold between 2009 and 2012. Although this amino acid was still only present in 2.8% of pandemic H1N1 isolates in 2012, it should be included in influenza surveillance due to its association with virulence in the mouse model.

In conclusion, deep sequencing combined with reverse genetics reveals that just two mutations (both in the HA gene segment) account for the difference between a wild type 2009-pandemic H1N1 virus and a cell culture-adapted high-growth strain. The mutations in the HA gene caused decreased receptor binding and HA trimer stability and were used to create a reverse genetics high titer strain that could be used for production of cell culture-based influenza virus vaccines.

Funding information

This work was supported by the German Ministry of Education and Research through the eBio project ViroSign (FK 0316180C), by the Austrian Science Foundation FWF (P25844) and by the German Research Foundation (HE 3763/15-1). P.H.S. thanks the Max-Planck Society for generous financial support. The funders had no role in study design, data collection and interpretation, or the decision to submit the work for publication

Acknowledgments

We thank Marina Drabkina, Kirstin Hoffmann, Jan-David Manntz and Jörg Angermann for excellent technical support, Christian Goosmann for help with EM, Ina Wagner and Hans-Joachim Mollenkopf for scanning the glycan arrays, Diane Schad for image editing and Rike Zietlow for editing the manuscript. The plasmid pHW2000 was donated by the St. Jude Children's Research Hospital, Memphis, TN, USA.

Appendix A. Supplementary material

Supplementary data associated with this article can be found in the online version at http://dx.doi.org/10.1016/j.virol.2016.02.002.

References

Bantia, S., Ghate, A.A., Ananth, S.L., Babu, Y.S., Air, G.M., Walsh, G.M., 1998. Generation and characterization of a mutant of influenza A virus selected with the neuraminidase inhibitor BCX−140. Antimicrob. Agents Chemother. 42, 801–807.

de Vries, R.P., de Vries, E., Martinez-Romero, C., McBride, R., van Kuppeveld, F.J., Rottier, P.J., Garcia-Sastre, A., Paulson, J.C., de Haan, C.A., 2013. Evolution of the hemagglutinin protein of the new pandemic H1N1 influenza virus: maintaining optimal receptor binding by compensatory substitutions. J. Virol. 87, 13868–13877.

Elderfield, R.A., Watson, S.J., Godlee, A., Adamson, W.E., Thompson, C.I., Dunning, J., Fernandez-Alonso, M., Blumenkrantz, D., Hussell, T., Investigators, M., Zambon, M., Openshaw, P., Kellam, P., Barclay, W.S., 2014. Accumulation of human-adapting mutations during circulation of A(H1N1)pdm09 influenza virus in humans in the United Kingdom. J. Virol. 88, 13269–13283.

Evans, E., Ritchie, K., 1997. Dynamic strength of molecular adhesion bonds. Biophys. J. 72, 1541–1555.

Feng, S.Z., Jiao, P.R., Qi, W.B., Fan, H.Y., Liao, M., 2011. Development and strategies of cell-culture technology for influenza vaccine. Appl. Microbiol. Biotechnol. 89, 893–902.

Galloway, S.E., Reed, M.L., Russell, C.J., Steinhauer, D.A., 2013. Influenza HA subtypes demonstrate divergent phenotypes for cleavage activation and pH of fusion: implications for host range and adaptation. PLoS Pathog. 9, e1003151.

Gamblin, S.J., Haire, L.F., Russell, R.J., Stevens, D.J., Xiao, B., Ha, Y., Vasisht, N., Steinhauer, D.A., Daniels, R.S., Elliot, A., Wiley, D.C., Skehel, J.J., 2004. The structure and receptor binding properties of the 1918 influenza hemagglutinin. Science 303, 1838–1842.

Garcia-Alcalde, F., Okonechnikov, K., Carbonell, J., Cruz, L.M., Gotz, S., Tarazona, S., Dopazo, J., Meyer, T.F., Conesa, A., 2012. Qualimap: evaluating next-generation sequencing alignment data. Bioinformatics 28, 2678–2679.

Garrison E, M.G., 2012. Haplotype-based variant detection from short-read sequencing. arXiv Preprint **arXiv** 1207, 3907.

Garten, R.J., Davis, C.T., Russell, C.A., Shu, B., Lindstrom, S., Balish, A., Sessions, W.M., Xu, X., Skepner, E., Deyde, V., Okomo-Adhiambo, M., Gubareva, L., Barnes, J., Smith, C.B., Emery, S.L., Hillman, M.J., Rivailler, P., Smagala, J., de Graaf, M., Burke, D.F., Fouchier, R.A., Pappas, C., Alpuche-Aranda, C.M., Lopez-Gatell, H., Olivera, H., Lopez, I., Myers, C.A., Faix, D., Blair, P.J., Yu, C., Keene, K.M., Dotson Jr., P.D., Boxrud, D., Sambol, A.R., Abid, S.H., St George, K., Bannerman, T., Moore, A. L., Stringer, D.J., Blevins, P., Demmler-Harrison, G.J., Ginsberg, M., Kriner, P., Waterman, S., Smole, S., Guevara, H.F., Belongia, E.A., Clark, P.A., Beatrice, S.T., Donis, R., et al., 2009. Antigenic and genetic characteristics of swine-origin 2009 A(H1N1) influenza viruses circulating in humans. Science 325, 197–201.

Gen, F., Yamada, S., Kato, K., Akashi, H., Kawaoka, Y., Horimoto, T., 2013. Attenuation of an influenza A virus due to alteration of its hemagglutinin-neuraminidase functional balance in mice. Arch. Virol. 158, 1003–1011.

Genzel, Y., Fischer, M., Reichl, U., 2006. Serum-free influenza virus production avoiding washing steps and medium exchange in large-scale microcarrier culture. Vaccine 24, 3261–3272.

Herfst, S., Schrauwen, E.J., Linster, M., Chutinimitkul, S., de Wit, E., Munster, V.J., Sorrell, E.M., Bestebroer, T.M., Burke, D.F., Smith, D.J., Rimmelzwaan, G.F., Osterhaus, A.D., Fouchier, R.A., 2012. Airborne transmission of influenza A/H5N1 virus between ferrets. Science 336, 1534–1541.

Herrmann, A., Sieben, C., 2015. Single-virus force spectroscopy unravels molecular details of virus infection. Integr. Biol. 7, 620–632.

Hinterdorfer, P., Baumgartner, W., Gruber, H.J., Schilcher, K., Schindler, H., 1996. Detection and localization of individual antibody-antigen recognition events by atomic force microscopy. Proc. Natl. Acad. Sci. USA 93, 3477–3481.

Hoffmann, E., Neumann, G., Kawaoka, Y., Hobom, G., Webster, R.G., 2000. A DNA transfection system for generation of influenza A virus from eight plasmids. Proc. Natl. Acad. Sci. USA 97, 6108–6113.

Hoffmann, E., Stech, J., Guan, Y., Webster, R.G., Perez, D.R., 2001. Universal primer set for the full-length amplification of all influenza A viruses. Arch. Virol. 146, 2275–2289.
Hughes, M.T., Matrosovich, M., Rodgers, M.E., McGregor, M., Kawaoka, Y., 2000. Influenza A viruses lacking sialidase activity can undergo multiple cycles of replication in cell culture, eggs, or mice. J. Virol. 74, 5206–5212.
Imai, M., Watanabe, T., Hatta, M., Das, S.C., Ozawa, M., Shinya, K., Zhong, G., Hanson, A., Katsura, H., Watanabe, S., Li, C., Kawakami, E., Yamada, S., Kiso, M., Suzuki, Y., Maher, E.A., Neumann, G., Kawaoka, Y., 2012. Experimental adaptation of an influenza H5 HA confers respiratory droplet transmission to a reassortant H5 HA/H1N1 virus in ferrets. Nature 486, 420–428.
James, J.M., Zeiger, R.S., Lester, M.R., Fasano, M.B., Gern, J.E., Mansfield, L.E., Schwartz, H.J., Sampson, H.A., Windom, H.H., Machtinger, S.B., Lensing, S., 1998. Safe administration of influenza vaccine to patients with egg allergy. J. Pediatr. 133, 624–628.
Jimenez-Alberto, A., Alvarado-Facundo, E., Ribas-Aparicio, R.M., Castelan-Vega, J.A., 2013. Analysis of adaptation mutants in the hemagglutinin of the influenza A (H1N1)pdm09 virus. PLoS One 8, e70005.
Jonson, P.H., Petersen, S.B., 2001. A critical view on conservative mutations. Protein Eng. 14, 397–402.
Karlas, A., Machuy, N., Shin, Y., Pleissner, K.P., Artarini, A., Heuer, D., Becker, D., Khalil, H., Ogilvie, L.A., Hess, S., Maurer, A.P., Muller, E., Wolff, T., Rudel, T., Meyer, T.F., 2010. Genome-wide RNAi screen identifies human host factors crucial for influenza virus replication. Nature 463, 818–822.
Katz, J.M., Webster, R.G., 1992. Amino acid sequence identity between the HA1 of influenza A (H3N2) viruses grown in mammalian and primary chick kidney cells. J. Gen. Virol. 73, 1159–1165.
Kaverin, N.V., Gambaryan, A.S., Bovin, N.V., Rudneva, I.A., Shilov, A.A., Khodova, O. M., Varich, N.L., Sinitsin, B.V., Makarova, N.V., Kropotkina, E.A., 1998. Post-reassortment changes in influenza A virus hemagglutinin restoring HA-NA functional match. Virology 244, 315–321.
Keleta, L., Ibricevic, A., Bovin, N.V., Brody, S.L., Brown, E.G., 2008. Experimental evolution of human influenza virus H3 hemagglutinin in the mouse lung identifies adaptive regions in HA1 and HA2. J. Virol. 82, 11599–11608.
Klenk, H.D., Rott, R., Orlich, M., Blodorn, J., 1975. Activation of influenza A viruses by trypsin treatment. Virology 68, 426–439.
Koerner, I., Matrosovich, M.N., Haller, O., Staeheli, P., Kochs, G., 2012. Altered receptor specificity and fusion activity of the haemagglutinin contribute to high virulence of a mouse-adapted influenza A virus. J. Gen. Virol. 93, 970–979.
Krzywinski, M., Schein, J., Birol, I., Connors, J., Gascoyne, R., Horsman, D., Jones, S.J., Marra, M.A., 2009. Circos: an information aesthetic for comparative genomics. Genome Res. 19, 1639–1645.
Langmead, B., Salzberg, S.L., 2012. Fast gapped-read alignment with Bowtie 2. Nat. Methods 9, 357–359.
Lin, Y.P., Wharton, S.A., Martin, J., Skehel, J.J., Wiley, D.C., Steinhauer, D.A., 1997. Adaptation of egg-grown and transfectant influenza viruses for growth in mammalian cells: selection of hemagglutinin mutants with elevated pH of membrane fusion. Virology 233, 402–410.
Mair, C.M., Ludwig, K., Herrmann, A., Sieben, C., 2014. Receptor binding and pH stability-how influenza A virus hemagglutinin affects host-specific virus infection. Biochim. Biophys. Acta 1838, 1153–1168.
Mair, C.M., Meyer, T., Schneider, K., Huang, Q., Veit, M., Herrmann, A., 2014. A histidine residue of the influenza virus hemagglutinin controls the pH dependence of the conformational change mediating membrane fusion. J. Virol. 88, 13189–13200.
McKenna, A., Hanna, M., Banks, E., Sivachenko, A., Cibulskis, K., Kernytsky, A., Garimella, K., Altshuler, D., Gabriel, S., Daly, M., DePristo, M.A., 2010. The Genome Analysis Toolkit: a MapReduce framework for analyzing next-generation DNA sequencing data. Genome Res. 20, 1297–1303.
Morris, S.J., Sarkar, D.P., White, J.M., Blumenthal, R., 1989. Kinetics of pH-dependent fusion between 3T3 fibroblasts expressing influenza hemagglutinin and red blood cells. Measurement by dequenching of fluorescence. J. Biol. Chem. 264, 3972–3978.
Murakami, S., Horimoto, T., Ito, M., Takano, R., Katsura, H., Shimojima, M., Kawaoka, Y., 2012. Enhanced growth of influenza vaccine seed viruses in vero cells mediated by broadening the optimal pH range for virus membrane fusion. J. Virol. 86, 1405–1410.
Narasaraju, T., Sim, M.K., Ng, H.H., Phoon, M.C., Shanker, N., Lal, S.K., Chow, V.T., 2009. Adaptation of human influenza H3N2 virus in a mouse pneumonitis model: insights into viral virulence, tissue tropism and host pathogenesis. Microbes Infect. 11, 2–11.
Okonechnikov, K., Golosova, O., Fursov, M., team, U., 2012. Unipro UGENE: a unified bioinformatics toolkit. Bioinformatics 28, 1166–1167.
Otte, A., Sauter, M., Daxer, M.A., McHardy, A.C., Klingel, K., Gabriel, G., 2015. Adaptive mutations that occurred during circulation in humans of H1N1 influenza virus in the 2009 pandemic enhance virulence in mice. J. Virol. 89, 7329–7337.
Pan, C., Cheung, B., Tan, S., Li, C., Li, L., Liu, S., Jiang, S., 2010. Genomic signature and mutation trend analysis of pandemic (H1N1) 2009 influenza A virus. PLoS One 5, e9549.
Papp, I., Sieben, C., Sisson, A.L., Kostka, J., Bottcher, C., Ludwig, K., Herrmann, A., Haag, R., 2011. Inhibition of influenza virus activity by multivalent glycoarchitectures with matched sizes. Chembiochem 12, 887–895.
Peitsch, C., Klenk, H.D., Garten, W., Bottcher-Friebertshauser, E., 2014. Activation of influenza A viruses by host proteases from swine airway epithelium. J Virol **88**, 282–291.
Pereira, C.L., Geissner, A., Anish, C., Seeberger, P.H., 2015. Chemical synthesis elucidates the immunological importance of a pyruvate modification in the capsular polysaccharide of streptococcus pneumoniae serotype 4. Angew. Chem. Int. Ed. Engl. 54, 10016–10019.
Rankl, C., Kienberger, F., Wildling, L., Wruss, J., Gruber, H.J., Blaas, D., Hinterdorfer, P., 2008. Multiple receptors involved in human rhinovirus attachment to live cells. Proc. Natl. Acad. Sci. USA 105, 17778–17783.
Rice, P., Longden, I., Bleasby, A., 2000. EMBOSS: the European molecular biology open software suite. Trends Genet. 16, 276–277.
Sieben, C., Kappel, C., Zhu, R., Wozniak, A., Rankl, C., Hinterdorfer, P., Grubmuller, H., Herrmann, A., 2012. Influenza virus binds its host cell using multiple dynamic interactions. Proc. Natl. Acad. Sci. USA 109, 13626–13631.
Smith, G.J., Vijaykrishna, D., Bahl, J., Lycett, S.J., Worobey, M., Pybus, O.G., Ma, S.K., Cheung, C.L., Raghwani, J., Bhatt, S., Peiris, J.S., Guan, Y., Rambaut, A., 2009. Origins and evolutionary genomics of the 2009 swine-origin H1N1 influenza A epidemic. Nature 459, 1122–1125.
Sriwilaijaroen, N., Suzuki, Y., 2012. Molecular basis of the structure and function of H1 hemagglutinin of influenza virus. Proc. Jpn. Acad. Ser. B Phys. Biol. Sci. 88, 226–249.
Steinhauer, D.A., 1999. Role of hemagglutinin cleavage for the pathogenicity of influenza virus. Virology 258, 1–20.
Takeuchi, M., Takasaki, S., Miyazaki, H., Kato, T., Hoshi, S., Kochibe, N., Kobata, A., 1988. Comparative study of the asparagine-linked sugar chains of human erythropoietins purified from urine and the culture medium of recombinant Chinese hamster ovary cells. J. Biol. Chem. 263, 3657–3663.
Vainer, B., Nielsen, O.H., Horn, T., 1998. Expression of E-selectin, sialyl Lewis X, and macrophage inflammatory protein-1alpha by colonic epithelial cells in ulcerative colitis. Dig. Dis. Sci. 43, 596–608.
Wagner, R., Matrosovich, M., Klenk, H.D., 2002. Functional balance between haemagglutinin and neuraminidase in influenza virus infections. Rev. Med. Virol. 12, 159–166.
Wildling, L., Rankl, C., Haselgrubler, T., Gruber, H.J., Holy, M., Newman, A.H., Zou, M. F., Zhu, R., Freissmuth, M., Sitte, H.H., Hinterdorfer, P., 2012. Probing binding pocket of serotonin transporter by single molecular force spectroscopy on living cells. J. Biol. Chem. 287, 105–113.
Wildling, L., Unterauer, B., Zhu, R., Rupprecht, A., Haselgrubler, T., Rankl, C., Ebner, A., Vater, D., Pollheimer, P., Pohl, E.E., Hinterdorfer, P., Gruber, H.J., 2011. Linking of sensor molecules with amino groups to amino-functionalized AFM tips. Bioconjug. Chem. 22, 1239–1248.
Wu, E.Y., Walsh, A.R., Materne, E.C., Hiltner, E.P., Zielinski, B., Miller 3rd, B.R., Mawby, L., Modeste, E., Parish, C.A., Barnes, W.M., Kermekchiev, M.B., 2015. A conservative isoleucine to leucine mutation causes major rearrangements and cold sensitivity in KlenTaq1 DNA polymerase. Biochemistry 54, 881–889.
Xu, R., McBride, R., Nycholat, C.M., Paulson, J.C., Wilson, I.A., 2012. Structural characterization of the hemagglutinin receptor specificity from the 2009 H1N1 influenza pandemic. J. Virol. 86, 982–990.
Xu, X., Nagarajan, H., Lewis, N.E., Pan, S., Cai, Z., Liu, X., Chen, W., Xie, M., Wang, W., Hammond, S., Andersen, M.R., Neff, N., Passarelli, B., Koh, W., Fan, H.C., Wang, J., Gui, Y., Lee, K.H., Betenbaugh, M.J., Quake, S.R., Famili, I., Palsson, B.O., Wang, J., 2011. The genomic sequence of the Chinese hamster ovary (CHO)-K1 cell line. Nat. Biotechnol. 29, 735–741.